EFFECT OF POROUS LAYER THICKNESS ON FREE CONVECTION IN A 3D CUBICAL ENCLOSURE FILLED WITH TRIHYBRID-NANOFLUID AND SATURATED WITH POROUS MEDIUM

Younus JANABI[1] ,Tudor PRISECARU[2], Valentin APOSTOL[3]

A 3D computational simulation is performed to examine free convection thermal transfer within a cubical cavity filled with (Al_2O_3-Cu-MWCNT-based water) trihybrid-nanofluid, one central layer of trihybrid nanofluid, and two layers of porous media. Navier-Stokes equations are implemented to model the convection thermal transfer for the trihybrid-nanofluid layer, while the governing equation in porous media is solved by using the Darcy-Brinkmann model. The objective is to identify the most appropriate geometrical and physical characteristics that optimize the thermal transfer in a cooling system domain. Numerical solutions are obtained employing Finite element method (FEM). Key parameters are studied under different ranges, such as the Rayleigh number (Ra), Hartmann number (Ha), Darcy number (Da), solid volume fraction of nanoparticles, and porosity of the porous layer.

Keywords: heat generation, cubical enclosure, porous medium, trihybrid nanofluid, Nanoparticles.

1. Introduction

Because porous medium is met in a wide range of conditions, the scientific and technical communities have paid close attention to the investigation of thermal transfer in these systems. In addition, to being widespread in nature, porous medium is employed in many engineering applications such as (thermal insulation systems, geothermal energy extraction, packed bed reactors, and energy storage device [1]. Initially introduced by Choi [2], trihybrid-nanofluid is described as a combination of based fluid such as oil, water, ethylene with nanoparticles. The objective of this combination is to improve the thermal conductivity of the base fluids. The investigation of convection thermal transfer inside an enclosure employing porous media is a crucial problem in numerous industrial engineering applications, like cooling computer systems, ground-coupled heat pumps, heat exchangers, electronic equipment, and solar collectors.

[1]PhD Student, National University of Technology POLITEHNICA of Bucharest, Department of Thermotechnics, Thermal Machines and Refrigeration Systems email: younus.janabi90@gmail.com
[2] Professor, National University of Technology POLITEHNICA of Bucharest, Department of Thermotechnics, Thermal Machines and Refrigeration Systems, e-mail: tudor.prisecaru@upb.ro
[3] Professor, National University of Technology POLITEHNICA of Bucharest, Department of Thermotechnics, Thermal Machines and Refrigeration Systems, e-mail: valentin.apostol@upb.ro

Thansekhar and Anbu Meenakshi [3] investigated the cooling impact of pure water with nanofluid (Al_2O_3 base water) by employing both non-uniform and uniform heating techniques. The findings revealed that nanofluid with a volume fraction of nanoparticles 0.25% had a greater temperature control impact than other fluids. Xia et al. [4] produced two types of nanofluids, first TiO_2/water and second Al_2O_3/water. It was also demonstrated that rising the volume fraction of Al_2O_3 enhances thermal conductivity. Meanwhile, the cooling impact of nanofluid changes with the type of the cooling channel.

In CFD, single and two-phase simulation of the trihybrid nanofluid are used in two different scenarios. The first phase model makes the assumption that the volume fraction and temperature have no bearing on the trihybrid nanofluid´s physical characteristics [5,6,7,8,9,10]. The Brownian and thermophoresis impacts considered in the second simulation [11,12,13,14]. The current determination is novel because it examines the impacts of different sizes of the four isothermal heating blocks on laminar free convection within a 3D cubical enclosure, which is filled with a central layer of (Cu-Al_2O_3-MWCNT-based water) trihybrid-nanofluid and partially saturated with two layers of porous medium. The study examined the impact of various parameters, including nanoparticles concentration, Da, Ha, and Ra. Additionally, an analysis is conducted to determine the effects of flow and thermal transfer within the enclosure for three various thicknesses of the porous layers.

2. Computational geometry

The physical model examined in this work is displayed in Fig.1. The cooling temperature of the right and left walls is maintained at constant, whereas the other walls are insulated. The cavity is heated by four isothermal heat sources. There are three layers of fluid in the cavity: the central layer is a trihybrid nanofluid, while the first and last layers are porous media. The current investigation is predicted on the following assumptions: Laminar, steady, incompressible, and Newtonian. With the exception of density changes, all thermophysical parameters are assumed to remain unchanged. It is assumed that there is a thermal equilibrium between solid matrix and the trihybrid nanofluid filling pores. Thermophysical characteristics of pure water and nanoparticles are shown in Table 1.

Table 1

Thermophysical properties of pure water and nanoparticles [16,17]

Properties	Water	Al_2O_3	MWCNT	Cu
ρ (kg/m^3)	998.2	3970	2100	8933
k[W/(m.K)]	0.613	40	3000	400
cp [J/(kg.K)]	4182	765	669.28	385
ß [1/K]	21×10^{-5}	2.55×10^{-5}	4.2×10^{-5}	5×10^{-5}

Navier-Stokes formulations were employed to simulate the convection thermal transfer for trihybrid nanofluid layer, while the governing equation in porous slab was solved by using Darcy Brinkmann model. In the present application, models for fluid flow and heat transfer solved numerically using the Finite element method (FEM).

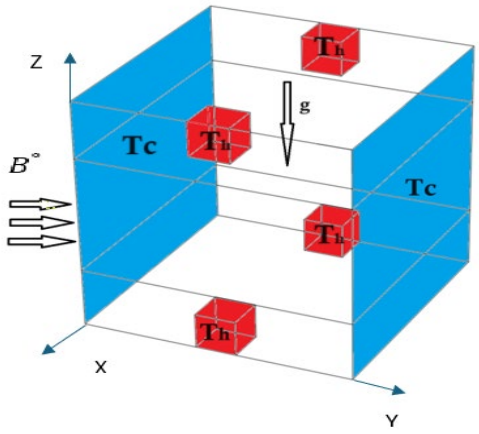

Fig.1: Schematic diagram of the present study.

3. Mathematical formulation

Under these assumptions the governing equation can be written:

The non-dimension form of the governing equations can be expressed as follows by using the dimensionless parameters [15,16].
Mass conservation equation:

$$\frac{\partial U}{\partial X}+\frac{\partial V}{\partial Y}+\frac{\partial W}{\partial Z}=0 \tag{1}$$

Momentum conservation equation for the X-direction:

$$\frac{1}{Cj}*\left(U\frac{\partial U}{\partial X}+V\frac{\partial U}{\partial Y}+W\frac{\partial U}{\partial Z}\right)=-\left(\frac{\rho_f}{\rho_{hnf}}\frac{\partial P}{\partial X}\right)*\frac{Ci}{Ci}+\frac{\mu_{hnf*\rho_f}}{\rho_{hnf*\mu_f}}*\frac{Pr}{Ci}*\left(\frac{\partial^2 U}{\partial X^2}+\frac{\partial^2 U}{\partial Y^2}+\frac{\partial^2 U}{\partial Z^2}\right)$$
$$-C_1\left(Pr*\frac{\mu_{hnf*\rho_f}}{\rho_{hnf*\mu_f}}*\frac{U}{Da}\right) \tag{2}$$

Momentum-Y

$$\frac{1}{Cj}*\left(U\frac{\partial V}{\partial X}+V\frac{\partial V}{\partial Y}+W\frac{\partial V}{\partial Z}\right)=-\left(\frac{\rho_f}{\rho_{hnf}}\frac{\partial P}{\partial Y}\right)*\frac{Ci}{Ci}+\frac{\mu_{hnf*\rho_f}}{\rho_{hnf*\mu_f}}*\frac{Pr}{Ci}*\left(\frac{\partial^2 V}{\partial X^2}+\frac{\partial^2 V}{\partial Y^2}+\frac{\partial^2 V}{\partial Z^2}\right)$$
$$-C_1\left(Pr*\frac{\mu_{hnf*\rho_f}}{\rho_{hnf*\mu_f}}*\frac{V}{Da}\right) \tag{3}$$

Momentum -Z

$$\frac{1}{Cj}*\left(U\frac{\partial W}{\partial X}+V\frac{\partial W}{\partial Y}+W\frac{\partial W}{\partial Z}\right)=-\left(\frac{\rho_f}{\rho_{hnf}}\frac{\partial P}{\partial Z}\right)*\frac{Ci}{Ci}+\frac{\mu_{hnf}*\rho_f}{\rho_{hnf}*\mu_f}*\frac{Pr}{Ci}*\left(\frac{\partial^2 W}{\partial X^2}+\frac{\partial^2 W}{\partial Y^2}+\frac{\partial^2 W}{\partial Z^2}\right)$$

$$-C_1\left(Pr*\frac{\mu_{hnf}*\rho_f}{\rho_{hnf}*\mu_f}*\frac{W}{Da}\right)\quad+C_1\left(\frac{\rho\beta)_{hnf}}{(\rho\beta)_f}\,Ra*\theta*Pr+Ha^2*Pr*W\right.$$

Energy equation (4)

$$U\frac{\partial\theta}{\partial X}+V\frac{\partial\theta}{\partial Y}+W\frac{\partial\theta}{\partial Z}=\alpha^*\left(\frac{\partial^2\theta}{\partial X^2}+\frac{\partial^2\theta}{\partial Y^2}+\frac{\partial^2\theta}{\partial Z^2}\right) \quad (5)$$

$$Ci=\begin{cases}1, & only\ trihybrid-nanofluid\\ e, & trihybrid-nanofluid\ with\ porous\end{cases}\qquad \alpha^*=\begin{cases}\alpha_{thnf}, & only\ trihybrid-nanofluid\\ \alpha_{eff}, & trihybrid\ nanofluid\ with\ porous\end{cases}$$

Equations (1) to (5) contain non-dimensional parameters, which can be defined as follows:

$$\theta=\frac{T-T_{ref}}{T_{hot}-T_{cold}},\quad T_{ref}=\frac{T_{cold}+T_{hot}}{2},\quad P=\left(\frac{pL^2}{\alpha^2\rho}\right),\quad Ra=\frac{\beta\Delta TgL^3}{v\alpha},\quad Ha=B_0H\sqrt{\frac{\sigma_f}{\mu_f}}$$

$$Da=\frac{k}{L^2},\qquad Pr_{fluid}=\frac{v_{fluid}}{\alpha_{fluid}} \quad (6)$$

Where e, v, α, and Pr represent the porosity of porous media, kinematic viscosity, thermal diffusivity, and Prandtl number, respectively.

The thermophysical characteristics of trihybrid are provided by [17,18].

The thermal diffusivity

$$\alpha_{eff}=k_{eff}/(\rho c_p)_{thnf} \quad (7)$$

$$k_{eff}=(1-e)k_s+e.k_{thnf} \quad (8)$$

Thermal diffusivity of trihybrid nanofluid:

$$\alpha_{thnf}=\frac{kt_{hnf}}{(\rho C_p)_{Al2O3-Cu-MWCNT/H2O}} \quad (9)$$

Dynamic viscosity of trihybrid nanofluid: the Einstein equation has been extended by Brinkman [9].

$$\emptyset_{thnf}=\emptyset_{Cu}+\emptyset_{Al2O3}+\emptyset_{MWCNT}$$

$$\mu_{thnf}=\frac{\mu_f}{(1-\emptyset_{thnf})^{2.5}} \quad (10)$$

Thermal conductivity on trihybrid nanofluid: the formulation of Maxwell [19].

$$\frac{k_{thnf}}{k_{hnf}}=\frac{k_3+(m-1)k_{hnf}-(m-1)\emptyset_3(k_{hnf}-k_3)}{k_3+(m-1)k_{hnf}+\emptyset_3(k_{hnf}-k_3)} \quad (11)$$

Density of trihybrid nanofluid:

$$\rho_{thnf}=\emptyset_{Al2O3}\rho_{Al2O3}+\emptyset_{Cu}\rho_{Cu}+\left(1-\emptyset_{thnf}\right)\rho_{bf}+\emptyset_{MWCNT}\rho_{MWCNT} \quad (12)$$

Specific capacity of Al2O3-Cu-MWCNT trihybrid nanofluid:[20]

$$(\rho C_p)_{thnf} = \emptyset_{Cu}(\rho C_p)_{Cu} + (1-\emptyset_{thnf})(\rho C_p)_{bf} + \emptyset_{Al2O3}(\rho C_p)_{Al2O3} + \emptyset_{MWCNT}(\rho C_p)_{MWCNT} \quad (13)$$

Volumetric expansion of trihybrid nanofluid:

$$(\rho\beta)_{thnf} = \emptyset_{Al2O3}(\rho\beta)_{Al2O2} + (1-\emptyset_{thnf})\rho\beta_f + \emptyset_{Cu}\rho\beta_{Cu} + \emptyset_{MWCNT}\rho\beta_{W_{MCNT}} \quad (14)$$

Electric conductivity of trihybrid nanofluid:

$$\sigma_{thnf} = \sigma_f\left[\frac{\sigma\emptyset_{Al2O3}+\sigma\emptyset_{Cu}+\sigma\emptyset_{MWCNT}+\sigma_f\emptyset_{thnf}+2\emptyset_{thnf}(\sigma\emptyset_{Al2O3}+\sigma\emptyset_{Cu}+\sigma\emptyset_{MWCNT}-\sigma_f\emptyset_{thnf})}{\sigma\emptyset_{Al2O3}+\sigma\emptyset_{Cu}+\sigma\emptyset_{MWCNT}+\sigma_f\emptyset_{thnf}-\emptyset_{thnf}(\sigma\emptyset_{Al2O3}+\sigma\emptyset_{Cu}+\sigma\emptyset_{MWCNT}-\sigma_f\emptyset_{thnf})}\right] \quad (15)$$

4. Boundary conditions

The subsequent expression gives boundary conditions for the ongoing examination.

For cold walls: U′=0, V′=0, W′=0,$\theta = 0$, and $\Phi = 0$ (16)

For all insulated walls (adiabatic): U′=0, V′=0, W′=0, and $\frac{\partial\theta}{\partial n} = 0$, (17)

At four heating sources: U′=0, V′=0, W′=0,$\theta = 1$, and $\Phi = 1$ (18)

Nusselt Number (Nu)

For a trihybrid nanofluid at an isothermal heating block, the Nu is described as the integral of the thermal flux across a wall.

$$Nu_{local} = \left(\frac{k_{thn}}{k_f}\right)\left(\frac{\partial\theta}{\partial x}\right)|_{=0,1} \quad (19)$$

The local Nusselt number, while the average Nusselt number is written as fo

$$Nu_{ave} = \iint_0^1 Nu\,.\,dY.dZ \quad (20)$$

5. Results and discussion

5.1 Impact of Darcy numbers on isotherms and streamlines

The impact of the Darcy number on the isotherm contours and streamline contours is displayed in Fig 2. The figure demonstrates that the isotherm and streamline patterns inside the enclosure are greatly impacted by the size of heaters and the Da. For small value of the Da=10^{-5}, we can observe that there is so slight

penetration of the trihybrid-nanofluid in case 1 and case 3, while in case 2 there is no infiltration of the trihybrid nanofluid into porous layer. It can also be noted that the main cells do not exist in the porous layers, while they are present in the trihybrid layer. The phenomenon occurs because the porous media, with a low value of Darcy number, presents great resistance to the trihybrid nanofluid motion, which is why the velocities are suppressed in the porous layers. Therefore, because there is not much flow into the porous medium layer, circulation inside the trihybrid nanofluid layer could become more intense. When the Darcy number increases to 10^{-3}, and 10^{-1}, it can be demonstrated that there is a significant change. This is the immediate outcome of the raised permeability of the porous medium thickness, which enables for larger amounts of trihybrid nanofluid flow infiltration.

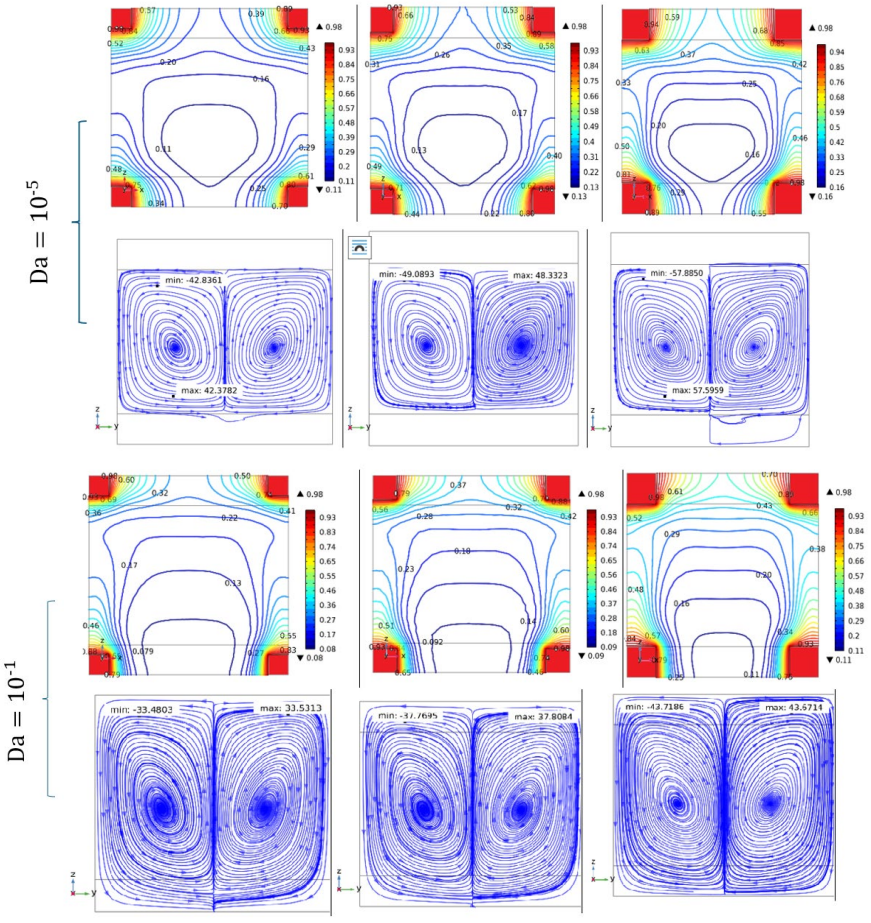

Fig. 2. Isotherms (top) and streamlines(bottom) for different Darcy numbers at Ha=30, Pr=6.2, kss=0.85, $\delta = \left(\frac{0.3}{2}\right) \emptyset = 0.2, Ra = 10^6$, and e=0.4.

This is shown by the |Vmax|, where the Darcy numbers case1 (Da=10^{-5}, 10^{-3},10^{-1}), the percentage values are 42.3782%, 36.5379%, and 33.5313%, respectively. Case 1 has stronger cell circulation than case 2 and case 3 based on the |Vmax|. The isotherms are shown in Fig.2. We can observe that there is slightly less difference in the behavior of isotherm contours in the three cases. However, the temperature within the enclosure decreases with an increase in a reduction in the size of the isothermal heating blocks and a reduction in the Da number value. As the value of the Darcy number rises, convection flow proceeds in the direction of the porous layer.

5.2 Velocity distribution

Fig.3 shows the influence of the thickness of the porous layer on the components of the velocity U, V, and W along the centerline X-axis at y=0.5, with constant parameters:Ø=0.2,δ=0.3/2, Ra=10^{6}, Da=10^{-3}, e=0.4, kss=0.85, Ha=20, and Pr=6.2. In the figure, it can be noted that the thickness of the porous layer has significant impact on the behavior of the velocity components. It has been shown that the highest velocity occurs with smaller thickness of the porous medium (δ=0.15/2) in all components (U, V, and W). When the thickness of porous medium is increased to δ=0.25/2, the velocity components gradually decrease, with maximum velocity reaching 110 in component W. As the porous layer thickness is further increased to δ=0.3/2, it can be observed that the velocity components decrease further, with the velocity in the W components dropping to 100. In the final analysis, because the smaller porous layer (δ=0.15/2) creates less obstacle to the trihybrid-nanofluid´s flow, a greater velocity is achievable. The resistance to flow rises with rising thickness of the porous layer, reducing the maximum velocity. When the porous layers are less thick, the flow becomes less constrained, which enhances the performance of the entire system.

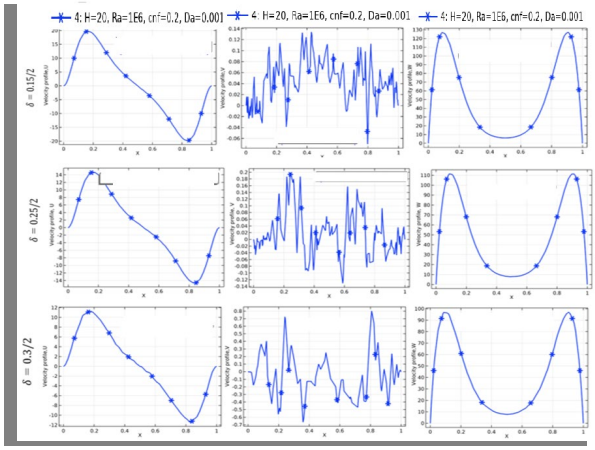

Fig.3. The impact of the porous layer thickness on the velocity profile along the centerline X -axis at y=0.5.

5.3Temperature distribution

The impact of the isothermal heat source sizes on the non-dimensional temperature profile along the horizontal centerline of the X-axis is demonstrated in Fig.4. It can be noted that the minimum temperature occurs at the center of the enclosure for the three cases. The figure shows clearly the effect of the heater sizes on the dimensionless temperature profile, with the minimum temperature peak occurring in case 1, while the maximum temperature peak is observed in case 3. Larger isothermal heat source size case 3 release heat over a greater surface area. If the trihybrid-nanofluid´s capacity to transfer heat decreases, this may result in elevated localized temperatures at the isothermal heat source surface, although the first impression that it would decrease the temperature. This is due to thermal concentration greater at the surface of the larger size of the isothermal heat source which means it takes longer for heat to disperse into the surrounding trihybrid -nanofluid.

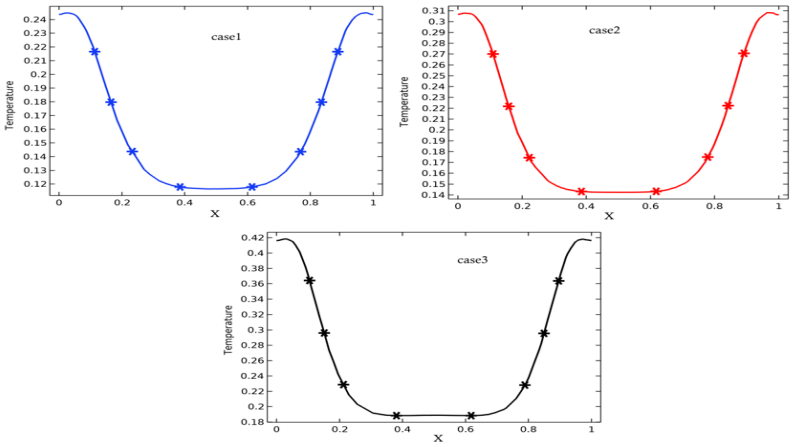

Fig.4: Variation of dimensionless temperature profile along horizontal along centerline of X-axis for different isothermal heat source sizes at $\emptyset = 0.2, \delta = \frac{0.3}{2}, e = 0.4, Da = 10^{-3}, kss = 0.85, Ra = 10^{6} and\ Pr = 6.2$

It is essential to highlight that the thermal boundary layer generally gets thicker in bigger isothermal heat sources, lowering the efficiency of the trihybrid-nanofluid close to the isothermal heat source surface in convection thermal away. Since heat accumulates within the boundary layer due to this diminished convection thermal transmission, the temperature increases close to the surface. On the other hand, smaller isothermal heat source case 1 has a greater flow of heat, which allows heat to spread into trihybrid-nanofluid faster. The thermal circulates more precisely and is more effectively dissipated by the surrounding

trihybrid-nanofluid, resulting in a cooler temperature adjacent to the isothermal heat surface.

5.4Average Nusselt number

5.4.1 Impact of the porosity

Table 3.

Specific measure of different sizes of heat source.

Case1	Heating source size =6. (0,1.0,1) cm
Case2	Heating source size =6. (0,12.0,12) cm
Case3	Heating source size =6. (0,15.0,15) cm

Fig.5 depicts the impact of porosity on the average Nusselt number for various sizes of heating source at Ha=20, Pr=6.2, Da=10^{-3}, Ø=0.2, Ra=10^{6},δ=0.3/2, and kss=0.85. It can be observed that the Nu_{ave} increases with rising porosity of the porous medium from (0.2 to 0.8). Additionally, the highest amount of Nu_{ave} occurs in case1, while the minimum value is found in case3.

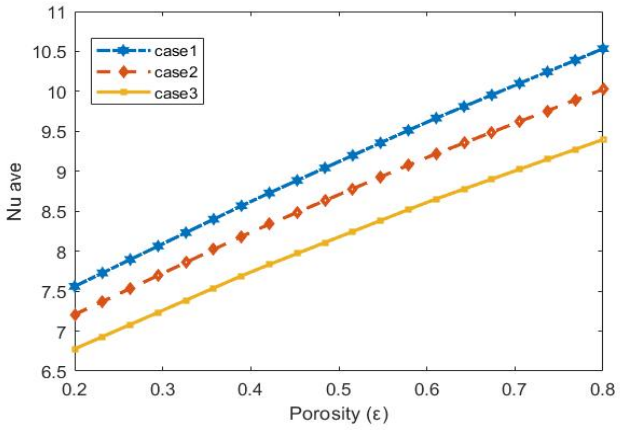

Fig.5. Variation of the Nu with porosity for various size of heater source.

This is increasing in the Nu_{ave} due to combinations of decreased thermal resistance, enhanced flow dynamic, improved surface area, as well as adjustments to the fluid-solid system´s efficient thermal characteristics. The reason for the increased value of the average Nu in case1 is because of the maximum ratio of surface area to volume. This rise in ratio leads to more effective thermal transfer, which improves the average Nusselt number.

5.4.2 Impact of heat generation

Fig.6 illustrates the impact of heat generation on Nu_{ave} for different isothermal heat source sizes at various constant parameters. We can observe that as the value of heat generation increases from (0 to 18), the heat transfer decreases gradually for all sizes of the isothermal heat source. Due to a thicker thermal boundary layer caused by higher temperatures generation, which also raises the temperature of the trihybrid-nanofluid close to the heated surface. This decreases the Nu_{ave} and reduces the driving force for thermal transfer by decreasing the variation in temperature between the trihybrid-nanofluid and the wall. On other hand, a smaller size of isothermal heat source generates a greater temperature variation, a less thick thermal boundary layer, and better thermal transfer, all of which increase the Nu_{ave}.

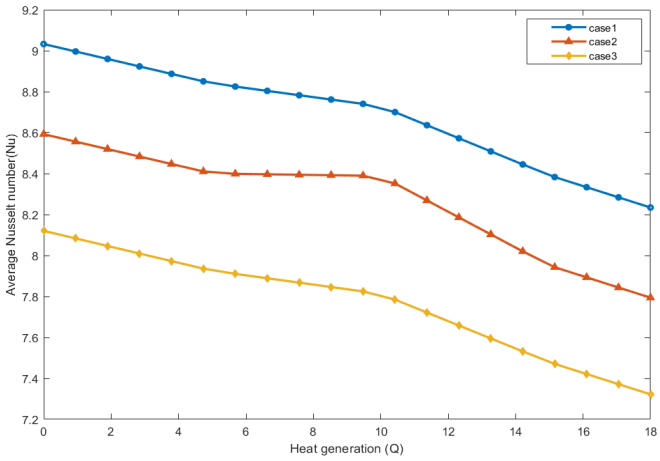

Fig.6. Variation of Nu_{ave} versus heat generation (Q) for different size of isothermal heat source at $\emptyset = 0.2, \delta = \frac{0.3}{2}, e = 0.4, Da = 10^{-3}, kss = 0.85, Ra = 10^{6} and\ Pr = 6.2$.

5.4.3 Impact of nanoparticle shape

The spherical shape of the nanoparticle (Cu-Al_2O_3-MWCNT-based water) trihybrid-nanofluid has been taken into account in the current investigation to clarify the previously described results. Nanoparticle shape has a major impact on the characteristics of thermal transfer within the enclosure. Fig.7 exhibits the impact of the nanoparticle shape factor on the Nu_{ave} for an isothermal heating block case 1 at ϕ=0.2, Ra=10^6, Da=10^{-3}, Pr=6.2, kss =0.85, $\emptyset$=0.2, and δ=0.3/2. The form factor n=3/ψ. The values of ψ are 0.36, 0.62, and 0.81 for blade, cylinder, and brick, respectively, as provided by Hamilton and Crosser [21] and Timoofeeva et.al [22]. It can be noted that the blade shape of the nanoparticles has a maximum Nu_{ave} number compared to other shapes as shown in Fig.7. These

outcomes imply that choosing the right nanoparticle shapes can greatly modify the thermal efficiency of trihybrid nanofluid, with brick, cylinder and blade shapes providing notable advantages in applications.

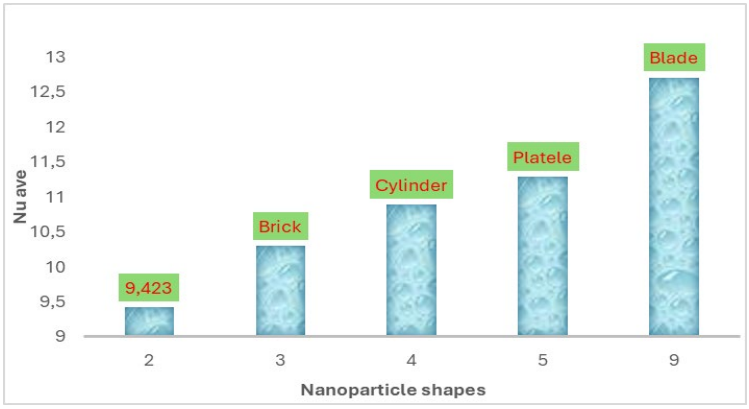

Fig.7. Nanoparticle shapes versus average Nusselt number at d= case 1.

5.4.4 Impact of nanoparticles concentration (Cu-Al_2O_3-MWCNT) on the Nu_{ave}

The figure shows that adding nanoparticles (Cu-Al_2O_3-MWCNT) to a base water enhances the heat conductivity of the water. This develops because the thermal conductivities of (Cu-Al_2O_3-MWCNT) are generally higher compared to that of pure water. Improved heat performance arises from the system being able to transmit a greater amount of heat with a similar amount of energy input. A higher average Nusselt number (Nu) results from this, indicating greater thermal transfer. The highest thermal transfer occurs in case 1 for each value of nanoparticle concentration, while the minimum value occurs in case 3 for all values of the nanoparticle concentration.

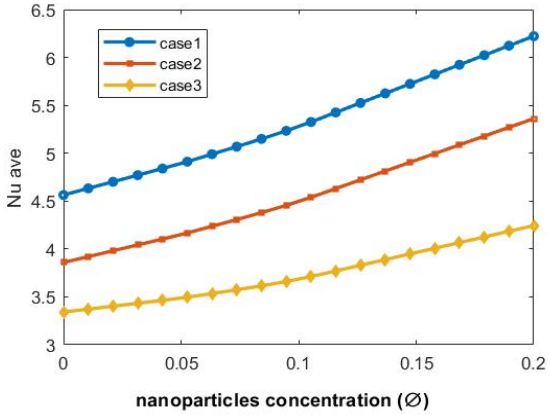

Fig.8. Variation of average Nusselt (Nu) versus nanoparticles concentration for different isothermal heat source at at $\emptyset = 0.2, \delta = \frac{0.3}{2}, e = 0.4, Da = 10^{-3}, kss = 0.85, Ra = 10^6 and\ Pr = 6.2$

6. Conclusions

This work involves the computational simulation of natural convection within a cubical enclosure that is partially saturated with porous medium and occupied with a Cu-Al_2O_3-MWCNT-based water trihybrid-nanofluid. The cavity is uniformly heated to a constant temperature (T_h), using four isothermal heating blocks and is cooled from the front and back at a uniform temperature (T_c). The remining boundaries are designed to prevent thermal exchange. The Porous layers are positioned at the upper and lower side of the enclosure, while the trihybrid nanofluid is positioned in the middle of the enclosure. The outcomes of the current study have been summarized.

1. The average Nusselt number elevates with improving porosity of the porous medium from (0.2 to 0.8).
2. The blade shape of the (**Cu-Al_2O_3-MWCNT**) has the highest Nu_{ave} compared to other shapes.
3. Adding nanoparticles (**Cu-Al_2O_3-MWCNT**) to a base water enhances the heat conductivity of the pure water
4. The temperature inside the cavity decreases with an elevate in the magnitude of the Darcy number and a reduction in the size of the isothermal heating blocks.
5. Case 1 has stronger cell circulation than case 2 and case 3 based on the Vmax|.
6. A greater Darcy number indicates that there is less resistance to convection flow from trihybrid-nanofluid into porous layer.
7. The maximum velocity occurs with smaller thickness of the porous medium (δ=0.15/2) in all components (U, V, and W)

Nomenclature

Ra	Rayleigh number (Ra=Gr*Pr)
Ha	Hartmann number
Da	Darcy number
k_{thn}	thermal conductivity of trihybrid
e	porosity of the porous media
Nu	Nusselt number
g	acceleration because of gravity (m/s^2)
U,V,W	Velocity components
Pr	Prandtl number
f	Fluid
thnf	trihybrid-nanofluid
Al_2O_3	Aluminum oxide (nanoparticle)
Cu	Copper (nanoparticle)
MWCNT	Multi-Walled Carbon Nanotubes (nanoparticle)
TiO_2	Titanium Dioxide (nanoparticle)
β	Thermal expansion coefficient
ρ	Density

σ	Electrical conductivity of the fluid
θ	Dimensionless temperature
μ	Dynamic viscosity

REFERENCES

[1] *Choi, S. U., & Eastman, J. A. (*1995). Enhancing thermal conductivity of fluids with nanoparticles (No. ANL/MSD/CP-84938; CONF-951135-29). Argonne National Lab.(ANL), Argonne, IL (United States).

[2] *Esfe, M. H., Barzegarian, R., & Bahiraei, M. (2020*). A 3D numerical study on natural convection flow of nanofluid inside a cubical cavity equipped with porous fins using two-phase mixture model. Advanced Powder Technology, 31(6), 2480-2492.

[3] *Anbumeenakshi, C., & Thansekhar, M. R. (2017*). On the effectiveness of a nanofluid cooled microchannel heat sink under non-uniform heating condition. Applied Thermal Engineering, 113, 1437-1443.

[4] *Xia, G. D., Liu, R., Wang, J., & Du, M. (2016).* The characteristics of convective heat transfer in microchannel heat sinks using Al2O3 and TiO2 nanofluids. International Communications in Heat and Mass Transfer, 76, 256-264.

[5] *Xuan, Y., & Roetzel, W. (2000*). Conceptions for heat transfer correlation of nanofluids. International Journal of heat and Mass transfer, 43(19), 3701-3707.

[6] *Xuan, Y., & Li, Q.* (2000). Heat transfer enhancement of nanofluids. International Journal of heat and fluid flow, 21(1), 58-64.

[7] *Elsheikh, A. H., Sharshir, S. W., Mostafa, M. E., Essa, F. A., & Ali, M. K. A.* (2018). Applications of nanofluids in solar energy: a review of recent advances. Renewable and Sustainable Energy Reviews, 82, 3483-3502.

[8] *Xu, H. J., Xing, Z. B., Wang, F. Q., & Cheng, Z. M*. (2019). Review on heat conduction, heat convection, thermal radiation and phase change heat transfer of nanofluids in porous media: Fundamentals and applications. Chemical Engineering Science, 195, 462-483.

[9] Wen, D., Lin, G., Vafaei, S. and Zhang, K. (2009), "Review of nanofluids for heat transfer applications", Particuology, Vol. 7 No. 2, pp. 141-150.

[10] *Khanafer, K. and Vafai, K.* (2018), "A review on the applications of nanofluids in solar energy field",Renewable Energy, Vol. 123, pp. 398-406.

[11] *Motlagh, S.Y. and Soltanipour, H.* (2017), "Natural convection of Al2O3-water nanofluid in an inclinedcavity using Buongiorno's two-phase model", International Journal of Thermal Sciences,Vol. 111, pp. 310-320.

[12] *Garoosi, F., Garoosi, S. and Hooman, K.* (2014), "Numerical simulation of natural convection and mixed convection of the nanofluid in a square cavity using Buongiorno model", Powder Technology, Vol. 268, pp. 279-292.

[13] *Buongiorno, J.* (2005), "Convective transport in nanofluids", Journal of Heat Transfer, Vol. 128 No. 3,pp. 240-250.

[14] *Garoosi, F., Garoosi, S. and Hooman, K*. (2014), "Numerical simulation of natural convection and mixed convection of the nanofluid in a square cavity using Buongiorno model", Powder Technology, Vol. 268, pp. 279-292.

[15] *Liu, K., Wang, N., Pan, Y., Alahmadi, T. A., Alharbi, S. A., Jhanani, G. K., & Brindhadevi*, *K.* (2024). Photovoltaic thermal system with phase changing materials and MWCNT nanofluids for high thermal efficiency and hydrogen production. Fuel, 355, 129457.

[16] *Jena, S., & Mishra, M. K.* (2023). Entropy analysis of Cu-Al2O3 based hybrid and Cu based mono nanofluid flows through porous medium: A comparative study. Case Studies in Thermal Engineering, 50, 103463.

[17] *Sheikholeslami M, Gorji-Bandpy M, Ganji DD, et al.* Natural convection of nanofluids in an enclosure betweena circular and a sinusoidal cylinder in the presenceof magnetic field. Int Commun Heat Mass Transfer.2012;39(9):1435–1443.
[18] *Thirupatithumma Anwar O, Reddy S. Sheri* finite differentially heated square cavity utilizing nanofluids. Int. J Heat MassTransfer. 2007; 50:2002-2018.
[19] Brinkman, H. C. (1952). The viscosity of concentrated suspensions and solutions. Journal of chemical physics, 20(4), 571-571.
[20] *Maxwell, James Clerk.* A treatise on electricity and magnetism. Clarendon press, 1881.
[21] *Hamilton, R. L., & Crosser, O. K.* (1962). Thermal Conductivity of Heterogeneous Two-Component Systems. Industrial & Engineering Chemistry Fundamentals, 1(3), 187–191.
[22] *Timofeeva, E. V., Routbort, J. L., & Singh, D.* (2009). Particle shape effects on thermophysical properties of alumina nanofluids. Journal of applied physics, 106.